Conical intersections and semiclassical trajectories: Comparison to accurate quantum dynamics and analyses of the trajectories

Ahren W. Jasper and Donald G. Truhlar[a)]
Department of Chemistry and Supercomputing Institute, University of Minnesota, Minneapolis, Minnesota 55455-0431

(Received 2 September 2004; accepted 15 October 2004; published online 4 January 2005)

Semiclassical trajectory methods are tested for electronically nonadiabatic systems with conical intersections. Five triatomic model systems are presented, and each system features two electronic states that intersect via a seam of conical intersections (CIs). Fully converged, full-dimensional quantum mechanical scattering calculations are carried out for all five systems at energies that allow for electronic de-excitation via the seam of CIs. Several semiclassical trajectory methods are tested against the accurate quantum mechanical results. For four of the five model systems, the diabatic representation is the preferred (most accurate) representation for semiclassical trajectories, as correctly predicted by the Calaveras County criterion. Four surface hopping methods are tested and have overall relative errors of 40%–60%. The semiclassical Ehrenfest method has an overall error of 66%, and the self-consistent decay of mixing (SCDM) and coherent switches with decay of mixing (CSDM) methods are the most accurate methods overall with relative errors of ~32%. Furthermore, the CSDM method is less representation dependent than both the SCDM and the surface hopping methods, making it the preferred semiclassical trajectory method. Finally, the behavior of semiclassical trajectories near conical intersections is discussed. © *2005 American Institute of Physics.* [DOI: 10.1063/1.1829031]

I. INTRODUCTION

Conical intersections (CIs) are seams of intersections between electronic states that occur in $F-2$ dimensions,[1–3] where F is the number of internal degrees of freedom. There has been a renewed interest in CIs as recent experimental evidence[4–12] suggests confirmation of Teller's early prediction[13] that ''the transition probability for this type of crossing (the CI) may become quite considerable.'' Although this idea played a pivotal role in many qualitative discussions of organic photochemistry, recent theoretical and experimental work has allowed for a much better quantitative understanding. Using dimensional analysis, it has been shown that local minima in the electronic energy gap (along some path) are usually associated with nearby conical intersections.[14] The (re)emerging picture of dynamics involving coupled electronic states is one in which a conical intersection (or some set of geometries along a CI) plays a role analogous to that of a conventional transition state for single electronic-state reactions, and the lowest-energy point on the CI seam in the former assumes a role almost[15] as prominent as a saddle point (the lowest-energy point on a conventional transition state dividing surface) for the latter. Therefore a variety of computational tools for characterizing and identifying CIs and the topography of the surrounding coupled potential energy surfaces using electronic structure techniques have been developed.[16–20] CIs have been observed or inferred computationally for a variety of chemical systems from H_3 (Refs. 21–24) to large biological molecules.[25–33]

A key concept that has guided much discussion in organic photochemistry has been the role of CIs in ''funneling'' probability amplitude from an excited electronic state to a lower one, which is similar in some sense to a transition state gating the flux from reactants to products. However, before one pushes the analogy too far, it is useful to briefly contrast CIs in multielectronic state reactions and transition state dividing surfaces in electronically adiabatic reactions. CIs are of dimension $F-2$, whereas transition state dividing surfaces are of dimension $F-1$. Thus transition state dividing surfaces can be defined such that all reactive trajectories must cross them whereas only a vanishingly small fraction of trajectories actually pass through a conical intersection. Even with its higher dimensionality, only under limited circumstances does a transition state dividing surface and its immediate neighborhood completely dominate the dynamics, and often a careful treatment of the global potential energy surface is required. A similar situation is likely for conical intersections and coupled states, and the validation of practical methods for simulating global coupled-states dynamics in systems with conical intersections is the subject of this article. In addition to testing the validity of these simulation methods, we use them to gain further insight into the importance of the CI and how it serves as a funnel.

The number of fully-dimensional dynamical studies involving CIs (or more generally, electronically nonadiabatic chemistry) is limited, and one may cite the following two challenges: (1) obtaining reliable potential energies and their couplings (either by fitting an analytic set of potential energy surfaces[34–42] or by computing these energies on-the-fly,[43–51] which is called direct dynamics), and (2) accurately and ef-

a)Author to whom correspondence should be addressed. Electronic mail: truhlar@umn.edu

ficiently modeling the nuclear motion, where (2) requires a practical means of accomplishing (1). The first difficulty is not considered in the present paper. It is assumed that a set of potential energy surfaces and their couplings are readily available or computable (which is not unreasonable in light of recent progress in electronic structure theory), and attention is focused on (2).

The dynamics of systems with CIs has been studied using both accurate and approximate methods. Accurate quantum mechanical dynamics calculations for systems with intersections have been performed for triatomic systems[52–62] (which have three vibrational degrees of freedom) and for systems with more than three internal degrees of freedom using simplified potential energy surfaces.[63–69] A two-mode approximation may be made in which the remaining degrees of freedom are ''frozen,'' and the resulting two-dimensional problem is treated using wave packets.[70] Several two-dimensional model problems have also been studied using wave packets.[71–74] Two-dimensional models, though, however useful in examining properties of the CI, are incomplete as descriptions of polyatomic systems, and the application of full-dimensional quantum mechanics is limited by computational considerations.

Approximate methods, including those that are based on semiclassical trajectories (i.e., that combine classical trajectories with quantum mechanical ideas to strike a balance between accuracy and computational efficiency), have also been employed,[55–58,63,75–78] including direct dynamics studies with the goal of finding ''representative'' trajectories for the decay mechanism.[79] These studies provide qualitative insights into reaction mechanisms and have been useful in explaining experimentally observed results. In general, the semiclassical methods are not well-validated against more accurate calculations, and quantitative interpretations cannot be made with confidence.

We have previously tested and developed[52–57,75,77,80–89] several methods designed for coupled-states dynamics that are based on semiclassical trajectories[90–94] and that are designed to treat polyatomic systems in their full dimensionality. Because the methods are based in part on classical mechanics, validation is required and is one goal of this paper. We have recently tested[87,89] several semiclassical trajectory methods against accurate quantum dynamics using a series of full-dimensional, two-state, atom–diatom model systems. This set of benchmark test cases includes three systems[82] with avoided crossings of the Landau–Zener–Teller-type[95–97] and two systems[83] with extended regions of weak coupling of the Rosen–Zener–Demkov-type.[98–100] In this work, the set of benchmark test cases is extended to include systems with CIs.

The semiclassical trajectory methods that are considered are based on independent classical trajectories. We pursue methods whose computational cost is comparable with the computational cost associated with single surface (classical) molecular dynamics. Various more complicated methods involving coupled trajectories and classical trajectories ''dressed'' with Gaussians have been developed and applied.[101–110] In contrast to the methods studied here, many of these methods have not been well-tested against accurate quantal results for multidimensional systems, and the development of efficient and well-validated methods for coupled-states dynamics remains important.

A family of five model systems with CIs is presented in Sec. II, full-dimensional quantum mechanical scattering calculations are performed, and the quantal results are used to test and validate several semiclassical trajectory methods. Section III discusses various details of the quantum mechanical and semiclassical calculations. Section IV presents comparisons of the accurate quantum mechanical and semiclassical trajectory results, and Sec. V is a summary.

II. MODEL SYSTEMS WITH CONICAL INTERSECTIONS

The energetics of the triatomic two-state model systems are expressed in terms a symmetric diabatic potential energy matrix[81,88]

$$\mathbf{U}=\begin{pmatrix} U_{11} & U_{12} \\ U_{12} & U_{22} \end{pmatrix}, \tag{1}$$

where U_{11} and U_{22} are diabatic potential energy surfaces and U_{12} is the diabatic (scalar) coupling. Adiabatic energies (V_1 and V_2) may be obtained by diagonalizing **U**, and the nonadiabatic coupling vector **d** (the off-diagonal matrix element of the nuclear gradient operator in the electronic basis) may be obtained from **U** and its gradients with respect to the nuclear coordinates.[56] Note that when the system is defined in the diabatic representation, **d** is fully determined by the diabatic-to-adiabatic transformation, and fully-converged quantum mechanical results are independent of which electronic representation is used.[88,111–113] Approximate dynamical methods, such as many of the semiclassical trajectory methods presented in Sec. III may not be formally independent of the choice of electronic representation, and it is therefore useful to have the model PEMs defined for both the adiabatic and diabatic representations.

When generating electronic energies using electronic structure methods, adiabatic energies are typically computed; the nonadiabatic coupling **d** is more difficult to compute, but techniques exist.[114] Once these adiabatic quantities are known, it is not, in general, possible to transform to a strictly diabatic representation,[115–117] i.e., a representation that completely removes the nonadiabatic coupling **d**, as there is some ambiguity in the adiabatic-to-diabatic transformation due to the ''nonremovable'' nonadiabatic coupling. One often defines a quasidiabatic basis, in which this nonremovable coupling is minimized. The nonremovable coupling is likely to be small compared to the removable coupling[117] (which is singular at the CI), and in practice the former is often neglected. By defining the model systems presented here in diabatic representation, the nonremovable coupling is rigorously absent.

Five model systems with conical intersections (referred to collectively as the family of MCH systems) are presented, each of which models the atom–diatom scattering event

$$\mathrm{M}^{*}+\mathrm{CH}(v,j)\rightarrow\begin{cases} \mathrm{M}+\mathrm{CH}(v'',j'') \\ \mathrm{H}+\mathrm{MC}(v',j'), \end{cases} \tag{2}$$

TABLE I. Parameters used in the diabatic coupling for the five MCH model systems.

Parameter	WL	WB	SL	SB	TL
α (deg)	45	45	45	45	85
A (eV)	0.09	0.09	0.30	0.30	0.45
β_2 (a_0)	0.5	1.0	0.5	1.0	0.5

where the asterisk denotes electronic excitation, M, C, and H are model atoms (in particular C does not model carbon), and v and j are vibrational and rotational quantum numbers for the diatomic fragments.

The functional forms for the MCH PEMs are obtained by modifying the family of previously presented MXH systems,[82] which themselves are loosely based on a model of the LiFH system[118] but with a smaller adiabatic energy gap ($\sim$0.2 eV). The MXH and LiFH systems feature an avoided crossing, i.e., a seam of nonzero minimum adiabatic energy gaps. For the five MCH PEMs, U_{11} and U_{22} are set equal to those previously defined for the MXH systems.[82] Briefly, U_{11} is the sum of a bound HC diatomic interaction (based on the HF diatomic curve) and repulsive MC and MH interactions; U_{22} is an extended LEPS function[119–122] with parameters similar to those for the LiFH system. The classical equilibrium geometry for the M+HC molecular arrangement is defined as the zero of energy, and the energies of the classical equilibrium geometries for the M*+HC and H+MC molecular arrangements are 0.76 and 0.67 eV, respectively, i.e., the classical ground-state reaction M+HC$\rightarrow$H+MC is endoergic by 0.67 eV, and the reaction M*+HC$\rightarrow$H+MC is exoergic by 0.09 eV. The C+MH molecular arrangement is not accessible at the total energies considered in the present study.

The masses of the M, C, and H model atoms are 6.047, 2.016, and 1.008 amu, respectively. With these masses, the zero-point energies for the HC and MC diatoms are 0.304 and 0.148 eV, respectively.

The diabatic coupling U_{12} differs for each member of the MCH family of PEMs and is obtained by modifying the couplings used for the MXH cases. Specifically,

$$U_{12}=U'_{12}[(R_{\mathrm{MC}}-R^0_{\mathrm{MC}})\sin\alpha+(R_{\mathrm{HC}}-R^0_{\mathrm{HC}})\cos\alpha], \quad (3)$$

where R_{AB} is the distance from atom A to atom B, U'_{12} is the functional form of the coupling used for the MXH systems,

$$U'_{12}=A\exp\left[-\left(\frac{g_1-\rho_1}{\beta_1}\right)^4-\left(\frac{g_2-\rho_2}{\beta_2}\right)^2\right], \quad (4)$$

with

$$g_1=R'\cos\phi-r_{\mathrm{HC}}\sin\phi, \quad (5)$$

$$g_2=R'\sin\phi+r_{\mathrm{HC}}\cos\phi, \quad (6)$$

$R^0_{\mathrm{MC}}=3.14\,a_0$, $R^0_{\mathrm{HC}}=2.08\,a_0$, $\rho_1=3.0\,a_0$, $\rho_2=1.3\,a_0$, $\beta_1=3.0\,a_0$, $\phi=-15.7°$, and

$$R'=\tfrac{1}{3}\sqrt{6R^2_{\mathrm{MC}}+3R^2_{\mathrm{MH}}-2R^2_{\mathrm{HC}}}\,. \quad (7)$$

The remaining parameters (α,A,β_2) were varied to create five model PEFs labeled SL, WL, SB, WB, and TL; the values of the parameters are summarized in Table I. The parameterizations are given two-letter labels as follows: The first letter is W, S, and T for $A=0.09$, 0.30, and 0.45 eV, respectively, and the second letter is L and B for $\beta_2=0.5$ and $1.0\,a_0$, respectively. The parameterizations also differ in α, but an additional letter is not employed to indicate this difference. A similar scheme was used to label the MXH systems,[82] where W, S, L, and B were chosen to stand for ''weak,'' ''strong,'' ''localized,'' and ''broad.'' Thus, for example, SB denotes strong coupling over a broad region.

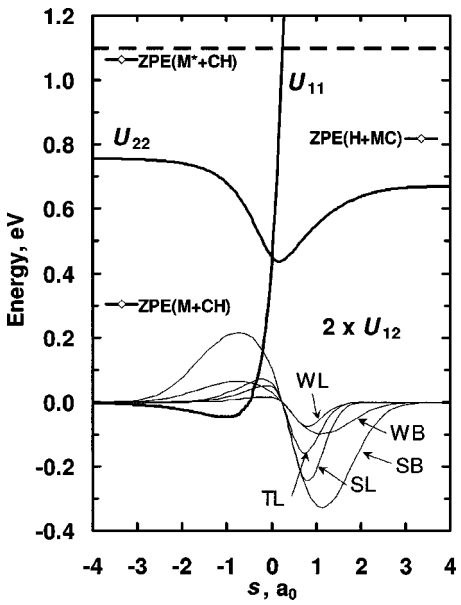

FIG. 1. Diabatic energies (thick solid lines) along the collinear minimum energy path s of U_{22}. The five MCH PEMs have different coupling surfaces U_{12} (thin solid lines), as indicated. Also shown are the zero-point energies of the asymptotic diatomic fragments (diamonds), and the total scattering energy (think dashed line).

The diabatic energies along the collinear minimum energy path of U_{22} are plotted in Fig. 1. All five MCH systems have the same U_{11} and U_{22} surfaces; the SL, WL, SB, WB, and TL parameterizations differ in the shape and magnitude of their diabatic coupling U_{12} as indicated in the figure. Also shown are the zero-point energies of the asymptotic diatomic fragments. Contour plots of the adiabatic and diabatic energies along with the magnitude of the nonadiabatic coupling are shown for the SL parameterization in Fig. 2.

Conical intersections occur at geometries where

$$U_{11}=U_{22} \quad (8)$$

and

$$U_{12}=0. \quad (9)$$

Each of these conditions is satisfied in a two-dimensional surface (for triatomic systems such as MCH), and the intersection of these surfaces forms (or, more exactly, may form) a one-dimensional seam of conical intersections. For the model MCH PEMs, the seam of CIs lies approximately in the direction of the MH stretching motion (or equivalently, along the M–C–H bending motion).

Conical intersections may be characterized[123,124] by identifying the two mass-weighted unit vectors $\hat{\mathbf{g}}$ and $\hat{\mathbf{h}}$ corresponding to the vectors

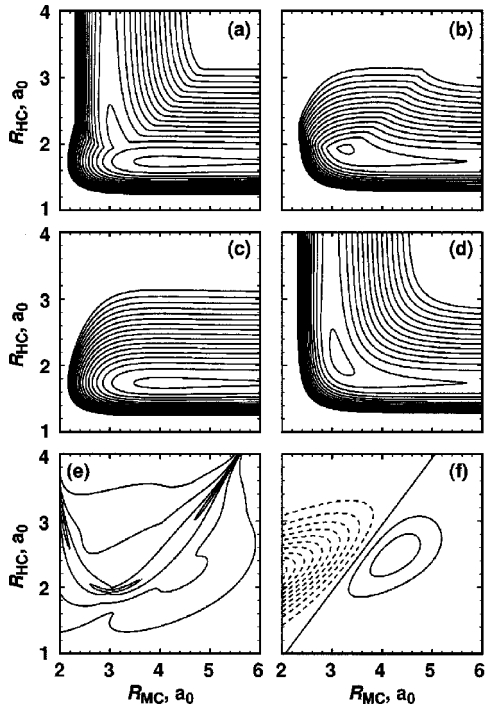

FIG. 2. Contour plots for the SL parameterization of collinear MCH. The contour spacing is 0.25 eV for (a) V_1, (b) V_2, (c) U_{11}, (d) U_{22}, and 0.025 eV for (f) U_{12}. The lowest-energy contour is 0.0 eV for panels (a) and (c) and 0.5 eV for panels (b) and (d). In panel (f), the $U_{12}=0$ contour is a straight line. Panel (e) shows the magnitude d of the nonadiabatic coupling, and contours are shown for 0.015, 0.15, 1.5, and 15 a_0^{-1}.

$$\mathbf{g} \equiv g\hat{\mathbf{g}} = \nabla(V_2 - V_1), \tag{10}$$

$$\mathbf{h} \equiv h\hat{\mathbf{h}} = (V_2 - V_1)\mathbf{d} \tag{11}$$

computed at some geometry along the CI, where $g=|\mathbf{g}|$, and $h=|\mathbf{h}|$. For the model PEMs, the geometry of the minimum-energy CI is at 180° for the M–C–H bond angle (collinear), and the energy of the CI is fairly constant as a function of bond angle from 100° to 180°. Over this range of bond angles, the unit vectors $\hat{\mathbf{g}}$ and $\hat{\mathbf{h}}$ both approximately correspond to an H–C stretching motion ($\hat{\mathbf{g}}\cdot\hat{\mathbf{h}} \approx 0.99$). The plane defined by $\hat{\mathbf{g}}$ and $\hat{\mathbf{h}}$ is called the $g-h$ plane or the ''intersection coordinate subspace,''[123] and an orthonormal set of unit vectors $\hat{\mathbf{g}}'$ and $\hat{\mathbf{h}}'$ (called ''intersection adapted coordinates''[124]) may be obtained by orthoganalizing $\hat{\mathbf{g}}$ and $\hat{\mathbf{h}}$ within the $g-h$ plane. We do this by setting $\hat{\mathbf{g}}'=\hat{\mathbf{g}}$ and rotating $\hat{\mathbf{h}}$. For the MCH systems, $\hat{\mathbf{h}}'$ approximately corresponds to an M–C stretching motion. Nuclear motions perpendicular to the intersection coordinate subspace preserve the conical intersection, whereas motions within the plane destroy either one or both of the conditions in Eqs. (10) and (11) and break the degeneracy.

Plots of the diabatic energies as functions of R_{HC} and R_{MC} for the SL parameterization are shown in Fig. 3. The CIs for these model systems are of the ''sloped'' type.[123] [A ''peaked'' CI would have surfaces similar to those in Fig. 3(a) along both $\hat{\mathbf{g}}'$ and $\hat{\mathbf{h}}'$.] Yarkony[124] has found the following quantities to be useful in characterizing CIs:

$$d_{gh}^2 = g^2 + h^2, \tag{12}$$

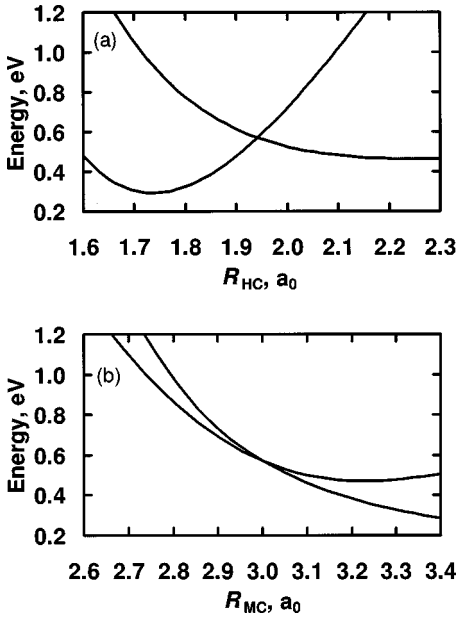

FIG. 3. Diabatic energies along (a) R_{HC} and (b) R_{MC} through the conical intersection at a M–C–H bond angle of 120°. In panel (a), R_{MC} is fixed at 1.94 a_0, and in panel (b), R_{HC} is fixed at 3.00 a_0.

$$\Delta_{gh} = (g^2 - h^2)/(g^2 + h^2), \tag{13}$$

$$s_g = \mathbf{s}\cdot\hat{\mathbf{g}}'/g, \tag{14}$$

$$s_h = \mathbf{s}\cdot\hat{\mathbf{h}}'/h, \tag{15}$$

where

$$\mathbf{s} \equiv \nabla(V_1 + V_2). \tag{16}$$

Nonzero values for s_g and s_h describe how the cone is tilted away from vertical, and a nonzero value of Δ_{gh} indicates that the cone does not have cylindrical symmetry. Values of the parameters defined by Eqs. (12)–(15) along with the energies and geometries along the CIs for the five MCH systems are presented in Table II. There is some diversity in the five systems, but all five systems are sloped cones with tilt parameters 0.6–1.2 and are asymmetric. The parameters ''predict'' that these cones will be less efficient than upright cones in trapping and disposing of the nuclear wave packet. We will return to this discussion in Secs. III.A and IV.C.

TABLE II. CI parameters for the MCH systems.

Parameter[a]	WL	WB	SL	SB	TL
d_{gh} (a_0 amu$^{1/2}$)	0.00177	0.00172	0.00172	0.00194	0.00160
Δ_{gh}	0.289	0.321	0.355	0.297	0.461
s_g	0.817	0.814	0.796	0.797	1.18
s_h	0.767	0.849	0.901	0.648	0.600
E_{CI}[b] (eV)	0.57	0.57	0.57	0.57	0.47
R_{HC} (a_0)	1.94	1.94	1.94	1.94	1.95
R_{MC} (a_0)	3.00	3.00	3.00	3.00	3.13
R_{MH} (a_0)	4.94	4.94	4.94	4.94	5.08

[a]The parameters d_{gh}, Δ_{gh}, s_g, and s_h were evaluated along the seam of CIs with the M–C–H bond angle fixed at 120°. The remaining parameters were evaluated at collinear geometries, which are the lowest-energy geometries along the seam of CIs.

[b]$E_{CI}=U_{11}=U_{22}=V_1=V_2$ at the CI.

In addition to the five parameterizations of the newly presented MCH system, we also consider three previously presented MXH parameterizations[82] (labeled SL, SB, and WL) and two previously presented YRH parameterizations[83] (labeled 0.1 and 0.2). The YRH system features noncrossing diabatic surfaces and weak coupling. Taken together, the set of MCH, MXH, and YRH model potential surfaces provides a qualitatively varied set of PEMs with which to study nonadiabatic dynamics and validate approximate semiclassical trajectory methods. Fully converged quantum mechanical calculations have previously been carried out for the MXH (Ref. 82) and YRH (Ref. 83) model systems and are presented for the MCH systems in Sec. III.

A set of six observables for the atom–diatom scattering event is considered: P_R, the probability of de-exciting and undergoing an atom-exchange (i.e., reacting); P_Q, the probability of de-exciting nonreactively (quenching); $P_N \equiv P_R + P_Q$, the total probability of de-excitation; $F_R \equiv P_R/P_N$, the fraction of de-excited trajectories that react; E'_{int}, the average final internal (rovibrational) energy of the de-excited reactive diatomic fragment; and E''_{int}, the average final internal (rovibrational) energy of the de-excited nonreactive diatomic fragment. The diatom is initially in its ground vibrational state, and the total angular momentum is zero. The total energy E (with respect to the classical minimum of the ground-state reactants) and initial rotational state j of the diatomic molecule are varied, and the initial conditions are labeled (E,j), where E is in eV. Final rovibrational energies are always measured with respect to classical equilibrium.

III. CALCULATIONS

III.A. Quantum mechanical calculations

Six-dimensional quantum mechanical calculations (three internal vibrations and three overall rotations) were carried out using the outgoing wave variational principle,[125–129] as implemented in the computer code VP,[130] and using the basis sets and numerical parameters previously used to obtain converged results for the MXH systems.[82] Calculations were carried out for all five MCH parameterizations at seven total energies from $E=1.07$ to 1.13 eV, where the zero of energy is at the classical minimum of the ground-state HC curve when HC is far from M. Convergence was demonstrated by comparing results from two calculations that differ in the number of basis functions (having 16614 and 20287 basis functions, respectively) and in their numerical parameters (see Ref. 82 for details). For example, at $E=1.10$ eV, there are 3 open channels for M*+HC, 23 open channels for M+HC, and 23 open channels for H+MC; thus there are 1225 unique state-to-state transition probabilities (for zero-total-angular-momentum atom-diatom collisions neglecting spin, a state is the same as a channel and is specified by a unique set of rovibrational quantum numbers and a label identifying molecular arrangement). For the SL parameterization at 1.10 eV, 96% of the transition probabilities are converged to better than 1% (these transition probabilities have an average value of 0.02), 3.5% are converged to between 1% and 5% (with an average value of 2×10^{-4}), and only three transition probabilities differ by more than 5% (with an average value of 10^{-5}). Similar convergence is obtained for all five MCH parameterizations at all of the scattering energies considered. The quantum mechanical results for the six observables discussed in Sec. II are converged to better than 1%.

TABLE III. Quantum mechanical results for the SL PEM for the M*+HC ($v=0$, $j=0$) collision.

E, eV[a]	P_R	P_Q	P_N	F_R	E'_{int}, eV	E''_{int}, eV
1.07	0.13	0.52	0.65	0.20	0.21	0.97
1.08	0.39	0.41	0.80	0.49	0.19	0.96
1.09	0.19	0.43	0.62	0.30	0.20	0.95
1.10	0.24	0.32	0.55	0.42	0.22	0.95
1.11	0.20	0.28	0.48	0.42	0.23	0.95
1.12	0.25	0.29	0.53	0.46	0.22	0.89
1.13	0.27	0.27	0.54	0.49	0.27	0.97
average	0.24	0.36	0.60	0.40	0.22	0.95

[a]Total energy with respect to the classical minimum of the isolated HC curve.

The quantum mechanical calculations were performed in the diabatic representation, thus avoiding complications associated with the geometric phase effect[131–137] when the adiabatic representation is used.

Quantum mechanical results often show significant dependence on total energy, even where the results of classical calculations do not. The quantum mechanical results are therefore averaged over energies from 1.07 to 1.13 eV to obtain average results for an interval centered at 1.10 eV. Quantum mechanical results for the SL model system are shown as a function of energy in Table III. The quantum results change significantly over this range, but the average values are close to those obtained at 1.10 eV. Similar energy dependencies were obtained for the other MCH parameterizations, and the average quantum mechanical results for the SL, SB, WL, WB, and TL parameterizations are summarized in Table IV.

We note that for the cones and scattering conditions considered here, only 29%–63% of probability density is de-excited by the cone, and the quantal results for P_N (de-excitation) and F_R (branching) may be roughly inversely correlated with the tilt of the cone $s^2=s_g^2+s_h^2$. A similar (but less strongly-correlated) relationship exists between the asymmetry of the cone Δ_{gh} and the observables P_N and F_R. These relationships agree with earlier speculations[123] and calculations[124] that cones that are more upright and symmetric are more efficient at de-exciting the system. Furthermore,

TABLE IV. Quantum mechanical results averaged over seven total energies from 1.07 to 1.13 eV for the five MCH parameterizations.

Observable	WL	WB	SL	SB	TL
P_R	0.46	0.45	0.24	0.15	0.13
P_Q	0.07	0.17	0.36	0.14	0.28
P_N	0.53	0.63	0.60	0.29	0.41
F_R	0.87	0.72	0.40	0.53	0.32
E'_{int}, eV	0.22	0.22	0.22	0.25	0.27
E''_{int}, eV	0.95	0.94	0.95	0.76	0.83

we find that these properties also enhance reactivity for the MCH systems.

III.B. Semiclassical trajectory calculations

Many semiclassical trajectory methods have been proposed, and we consider only those semiclassical trajectory methods that are well tested and that are based on the independent trajectory approximation, where an ensemble of trajectories is used to model the system and each trajectory evolves independently of the other trajectories in the ensemble.

The electronic motion is modeled using the ''classical path'' approximation for calculating the electronic state populations.[90,94,138,139] Briefly, the time-dependent electronic Schrödinger equation is solved along some classical trajectory. The solution for each trajectory may be represented in terms of the time evolution of an electronic state density matrix $\boldsymbol{\rho}$, where ρ_{11} is the electronic state population of state 1, for example, and ρ_{12} is an electronic state coherence. The time evolution of $\boldsymbol{\rho}$ depends on the nuclear velocity, the nonadiabatic vector coupling **d**, and the adiabatic energies (for the adiabatic representation) or on the diabatic energies (for the diabatic representation).

Semiclassical trajectory methods may be characterized by their treatment of the nonadiabatic transition. In the surface hopping approach,[85,90,138–141] trajectories evolve on the diagonal potential energy surfaces (e.g., the adiabats V_1 and V_2 or the diabats U_{11} and U_{22}, for two-state systems), and this single-surface propagation is interrupted by stochastic surface switches or hops. At a hopping event, the trajectory is placed on a different potential energy surface (if the transition is energetically allowed, as discussed below), an adjustment to the nuclear kinetic energy is made to conserve total energy, and propagation is continued.

Several schemes for computing the probability of hopping have been suggested. Using Tully's fewest-switches (FS) prescription[139] (sometimes called molecular dynamics with quantum transitions or MDQT), the hopping probability is obtained by monitoring the relative change in the classical path electronic state populations $\boldsymbol{\rho}$ and minimizing surface switches, as discussed elsewhere.[139] As in an earlier method,[138] hopping decisions are allowed all along the trajectory (not just at localized seams) at small time intervals (which may be taken to be the time-step of the integrator).

The FS prescription attempts to maintain electronic-nuclear self-consistency such that the fraction of trajectories in each electronic state matches the classical path electronic state populations. For many systems, however, the FS prescription may call for a surface hop to a higher-energy electronic state such that system is not allowed to hop by conservation of energy.[83,84,142,143] These so-called ''frustrated'' hops destroy the electronic-nuclear self-consistency, and their treatment can have a large effect on the results of a surface hopping simulation.[83,84] It has been suggested that these hops be ignored[143] (denoted by ''+'') or that the nuclear momentum along the nonadiabatic coupling vector be reflected[80,142,144] (denoted by ''−''). We have previously tested[83] these two approaches, along with several other approaches, and our studies led us to develop a method in which *some* frustrated hops are allowed to hop by incorporating time uncertainty into the hopping times[84] (we call this method FS with time uncertainty or FSTU). Those hops that are not allowed by time uncertainty may be treated using either the + or − prescriptions. We have also developed[85] a hybrid approach in which the + or the − prescription is used based on the gradient of the electronic surface toward which the trajectory is hopping (called the ∇V method). We have previously shown[84,85] that the FSTU∇V method is more accurate than several other methods tested. In this work, we consider the FSTU∇V method along with the FS− and FS+ methods.

Also considered in the present study is the surface hopping scheme of Parlant and Gislason,[145] which we call the exact-complete passage (ECP) method. In this method, hopping decisions are allowed only at locations along the classical trajectory where the magnitude of the nonadiabatic coupling vector **d** is a maximum, and the hopping probability is determined by integrating the total change in the classical path electronic state populations between local minima in the magnitude of **d**. At local minima in **d**, the electronic state density $\boldsymbol{\rho}$ is reinitialized. When classically forbidden hops are encountered, the + prescription is used. This method attempts to incorporate an explicit treatment of coherence and decoherence into trajectory surface hopping.

Another general approach to treating nonadiabatic events within the independent trajectory ensemble formalism involves propagating trajectories on average potentials, which are linear combinations of V_1 and V_2 or U_{11}, U_{12}, and U_{22}. We refer to these methods as self-consistent potential (SCP) methods. Several SCP methods have been proposed.[146–152] The semiclassical Ehrenfest (SE) method[146] is a simple SCP method in which trajectories propagate on a linear combination of the potential energy surfaces weighted by their classical path electronic state populations. For example, if the electronic state population is equally distributed in two electronic states, the trajectory propagates on a surface that is the arithmetic average of the two surfaces. Although this approach is formally appealing, the mean-field approximation suffers from serious problems. When the average potential is employed, trajectories may (and in general do) finish the simulation in mixed final states, giving internal and translational energies that do not correspond to any single isolated product. Furthermore, SE trajectories are not able to explore processes associated with small electronic probabilities, as every trajectory in the ensemble will be determined mainly by the potential energy surface associated with the high-probability event.[81,94] Because of the mixed state problem, there is some ambiguity in how to perform the final state analysis. In this work, we use the histogram method.[55]

The SE electronic density matrix along a given trajectory does not collapse to a pure state or an incoherent mixed state, and this may be interpreted[86,89] as a problem with the semiclassical treatment of decoherence within the SE formalism, i.e., a SE trajectory is fully coherent and a proper treatment requires some decoherence. We identify two sources of decay of the electronic state density matrix: dephasing, which is the tendency of the off-diagonal elements to go to zero, and demixing or decay of mixing (DM), which is the algo-

rithmic need for the SE trajectory (which represents a mixture of electronic states) to demix to an ensemble of single-surface trajectories representing physical product states.

A general set of DM equations (which also include dephasing) was obtained[86,153] by requiring first-order decay of the electronic state amplitudes and conservation of energy, angular momentum, and electronic phase angle. Briefly, the DM formalism collapses each mixed SE-like trajectory continuously toward some pure state K. The decoherent state K is determined stochastically using equations analogous to those used for the hopping probability in the fewest-switches surface hopping method. The remaining parameters to be specified are: (1) the direction $\hat{\mathbf{s}}$ in which energy is removed or deposited as the system demixes, and (2) the demixing time τ, where $1/\tau$ is the rate at which the system demixes to a pure state. We define $\hat{\mathbf{s}}$ such that $\hat{\mathbf{s}}$ points along the nonadiabatic coupling vector $\mathbf{d}$ when the magnitude of $\mathbf{d}$ is large, and $\hat{\mathbf{s}}$ points along the vibrational nuclear momentum otherwise. The optimal semiclassical rate of decoherence (or in this context, demixing) is not known and deserves continued study.[154,155] We have tested[86,87,89] a variety of simple prescriptions for τ, and we have taken (for a two-state system) the following expression as a reasonable one:

$$\tau = \frac{\hbar}{|E_1 - E_2|}\left(C + \frac{E_0}{(\mathbf{P}\cdot\hat{\mathbf{s}})^2/2\mu}\right), \tag{17}$$

where $E_i = V_i$ or U_{ii} for the adiabatic and diabatic representations, respectively, $\mathbf{P}$ is the nuclear momentum, μ is the reduced mass of the system (all coordinates are scaled to the same reduced mass when applying this formula), and C and E_0 are parameters. We have previously suggested[87,89] $C = 1$, and $E_0 = 0.1\,E_h$ ($1\,E_h = 27.211$ eV), and we have shown that the results are not overly sensitive to these parameters provided that the τ is large enough. Therefore in the present work we have used these values for all DM calculations.

We have developed three DM methods with varying degrees of coherence.[86,89,153] The natural decay of mixing[153] (NDM) method artificially enhances decoherence and will not be considered in this paper. The self-consistent decay of mixing[86] (SCDM) and coherent switches with decay of mixing[89] (CSDM) methods have both given good results, and both will be tested here. The SCDM method is ''locally coherent'' in the sense that no attempt is made to preserve the coherent motion over extended regions of the trajectory. The CSDM method is more coherent that the SCDM method. Specifically, in the CSDM method, the fully coherent SE equations of motion are used to compute the switching probability of the decoherent state K. Between regions of strong coupling, the electronic state density matrix $\boldsymbol{\rho}$ is partially collapsed to a dynamically decayed electronic state density matrix (and not necessarily to a pure state). See Ref. 89 for more details.

Semiclassical trajectory calculations consisting of 5000 trajectories were carried out using the NAT computer code.[156] Our implementation of the various semiclassical methods, the selection of initial conditions, the analysis of the final products, and additional computational details are described elsewhere.[55,56,86]

TABLE V. Semiclassical trajectory methods tested in this paper.

Method	Reference	Description
ECP	145	The ''exact complete passage'' surface hopping method of Parlant and Gislason
FS+	139	Tully's fewest switches surface hopping method, where the plus indicates that frustrated hops are ignored
FS−	142	Tully's fewest switches surface hopping method, where the minus indicates that at frustrated hops the nuclear momentum is reflected along the nonadiabatic coupling vector
FSTU∇V	84, 85	The fewest switches with time uncertainty method, where the ∇V indicates that frustrated hops are treated by the grad V method
SE	146	The semiclassical Ehrenfest self-consistent potential (SCP) method
SCDM	86	The self-consistent decay of mixing SCP method
CSDM	89	The coherent switches with decay of mixing SCP method

Table V summarizes the semiclassical methods tested in this paper.

III.C. Choice of electronic representation

The generalized Born–Oppenheimer approximation involves separating a subspace of electronic states from the rest. Having made this separation, the results should depend on the choice of subspace but not on the electronic basis with which it is spanned, i.e., no result should depend on whether the diabatic or adiabatic representation is used to represent the electronic states. Accurate quantum mechanical results are therefore independent of the choice of electronic representation; however, many approximate methods (including several of the semiclassical trajectory methods discussed above) do depend on the choice of electronic representation. Given a diabatic representation in which the electronic state coupling due to nuclear motion is either zero by definition (as in the systems studied here) or may be assumed to have a negligible effect (which is a reasonable assumption for real molecular systems, since these couplings can be completely removed by diabatic transformations in the vicinity of intersections and can be shown to have relatively small effects in regions where they cannot be removed),[88,115,117,157–160] it is a straightforward exercise to transform to an adiabatic representation, and so one may carry out the dynamics calculations in either representation. Therefore it is of considerable practical interest to consider the accuracy of the various semiclassical methods in both representations. The only semiclassical method (of the seven tested in the present work and summarized in Table V) that is formally independent of electronic representation is the SE method.[146] Surface hopping methods are often very dependent on representation,[83,87] and the decay of mixing methods are less dependent.[86,87,89]

An important question in developing and applying semiclassical theories is therefore: Which representation is the most accurate for a given system, set of conditions, and semiclassical theory? Actually, the situation is more complicated, as any single system may have certain regions where the adiabatic representation is preferred and other regions

where the diabatic representation is preferred, and this diversity within a given system is more likely to be encountered in complex applications of practical interest than in low-dimensional cases where testing against accurate quantal results is feasible. Thus, not only do we wish to find out which representation leads to more accurate results, we also want to find semiclassical methods that do not depend sensitively on the choice of representation. Such methods are in some sense closer to accurate quantum dynamics, and they are more likely to lead to accurate results for complex systems.

It has been suggested[94] that the adiabatic representation is the ideal representation for surface hopping. The argument may be presented by considering a two-state example, where U_{11} and U_{22} are the diabatic surfaces, V_1 and V_2 are the adiabatic surfaces, and $V_1 < V_2$. When the coupling is nonzero, the diabatic energies are always between the adiabatic energies. Trajectories running on the adiabatic surfaces are able to approximate the diabatic energies in some average sense (not the self-consistent SE average, but an algorithm-dependent ensemble average) by hopping back and forth, i.e., by having higher energies for some portion of the trajectory and then having lower energies. Diabatic trajectories, however, cannot approximate the adiabatic energies on average by hopping between the diabatic surfaces because U_{11} and U_{22} are both always less than V_2 and always greater than V_1. Another way to say this is that the best representation for surface hopping is the representation with the larger energy gap. This argument is physically reasonable, but for systems with conical intersections it might run counter to another kind of intuitive argument, namely that one should carry out the calculation in the representation that provides the best zero-order picture of the dynamics. Trajectories passing precisely through a conical intersection would be expected to be perfectly diabatic in zero order,[71] and although only an infinitesimal fraction of the trajectories will actually pass through the intersection, many trajectories will come close to it. And yet trajectories far from the intersection are expected to be adiabatic in zero order, so ultimately it is a system-dependent quantitative issue.

By comparing accurate quantum mechanical and semiclassical trajectory results, we have previously observed[57,81] that the diabatic representation may lead to more accurate semiclassical results for some systems, even systems without CIs. The Calaveras County (CC) criterion was developed[57,81] for estimating which representation is likely to be more accurate in the absence of quantum mechanical results. The CC representation is the representation in which surface hopping trajectories attempt the fewest number of hops, as estimated from a small set of calculations in both the adiabatic and diabatic representations. The CC criterion was previously shown[57] to successfully predict the most accurate representation for several test cases more often than several other criteria, and in subsequent work[86–89] we found that it continued to predict correctly, more often than not, which of the two representations (diabatic or adiabatic) would lead to more accurate results for a variety of semiclassical methods.

One may motivate the use of the CC representation for semiclassical trajectories as follows. Although it is true that the average value of the potential energy experienced by an adiabatic surface hopping trajectory may more closely approximate the average diabatic energies than vice versa, adiabatic surface hopping trajectories never propagate on that average surface. They propagate on one or the other of the two adiabatic surfaces, which themselves do not resemble the diabatic surfaces any more than the diabatic surfaces resemble the adiabatic surfaces. Adiabatic nuclear motion, therefore, does not approximate diabatic nuclear motion any better than diabatic motion approximates adiabatic motion. Furthermore, surface hops involve a somewhat arbitrary set of decisions about how to conserve total energy and suffer from self-consistency-violating frustrated hops. We conclude that the best representation is the representation in which the uncoupled surfaces (either adiabatic or diabatic) are the best approximation to the fully coupled system, i.e., if the diabatic surfaces are less coupled than the adiabatic surfaces, then the diabatic surfaces are a better first-order picture of the dynamics, fewer hops are required, and the diabatic representation is preferred. Tully has also suggested that the most accurate representation is the one that minimizes surface hops.[94] Furthermore the model that systems decohere to the electronic representation that is least coupled by the nuclear motion is consistent with quantum information theory, which states that the quantum subsystem decays to the eigenstates of an operator that commutes with the interaction between the quantal and classical subsystems.[161]

We have previously[81] identified the CC representations for the MXH and YRH test cases, and the CC representation and various hopping statistics for the MCH, MXH, and YRH systems are summarized in Table VI. All three of the YRH test cases strongly prefer the adiabatic representation, and three of the nine MXH cases prefer the diabatic representation. For the MCH cases, the adiabatic representation is preferred for the SB parameterization, whereas the diabatic representation is preferred (to varying degrees) for the remaining MCH parameterizations.

IV. RESULTS AND DISCUSSION

IV.A. Calaveras Country representation

ECP, FS+, FS−, FSTU∇V, SE, SCDM, and CSDM semiclassical trajectory calculations were carried out for all five MCH test cases to obtain the six observables discussed in Sec. II. In all cases errors are computed by comparing semiclassical calculations at 1.10 eV to the average quantum mechanical results in Table IV. Relative errors were computed and averaged over the five test cases as discussed elsewhere,[89] and results for the adiabatic (A), diabatic (D), and CC representations are summarized in Table VII. As discussed above, the SE method is formally independent of electronic representation. For all of the remaining methods except the ECP method, the D representation is more accurate overall than the A representation, and the CC representation is more accurate overall than either the A or D representations. There is a total of 30 observables (six observables for each of the five cases), and for the ECP, FS+, FS−, FSTU∇V, SCDM, and CSDM methods the CC representation predicts the most accurate representation for 17–20 of

TABLE VI. Hopping statistics per trajectory.[a]

				Successful hops		Frustrated hops		Total hopping attempts		
System	U_{12}[b]	I.C.[c]	CC rep	Adiabatic	Diabatic	Adiabatic	Diabatic	Adiabatic	Diabatic	Ratio A/D
YRH	0.1	(1.10,0)	A	0.16	1.9	0.29	8.0	0.45	10.	0.045
	0.2	(1.10,6)	A	0.18	1.0	0.11	2.6	0.29	3.6	0.079
		(1.02,0)	A	0.050	0.38	0.078	1.8	0.13	2.2	0.058
MXH	SB	(1.10,0)	A	2.6	5.0	1.6	5.9	4.2	11	0.39
		(1.10,1)	A	2.6	4.8	1.7	6.0	4.3	11	0.40
		(1.10,2)	A	2.6	4.9	1.7	6.2	4.3	11	0.39
	SL	(1.10,0)	A	2.3	1.8	1.1	2.5	3.4	4.3	0.79
		(1.10,1)	A	2.2	1.8	1.2	2.5	3.4	4.4	0.78
		(1.10,2)	A	2.2	1.8	1.1	2.4	3.3	4.3	0.78
	WL	(1.10,0)	D	2.4	0.35	0.44	0.67	2.8	1.0	2.8
		(1.10,1)	D	2.3	0.37	0.46	0.70	2.7	1.1	2.5
		(1.10,2)	D	2.1	0.35	0.42	0.65	2.6	1.0	2.6
MCH	WL	(1.10,0)	D	3.2	0.13	0.089	0.10	3.3	0.23	14
	WB	(1.10,0)	D	3.1	0.69	0.14	0.65	3.2	1.3	2.4
	SL	(1.10,0)	D	3.3	0.91	0.41	0.83	3.7	1.7	2.1
	SB	(1.10,0)	A	3.1	3.8	0.43	3.6	3.5	7.4	0.47
	TL	(1.10,0)	D	3.5	2.0	0.76	1.4	4.3	3.4	1.2

[a]Obtained using the FSTU∇V method. Similar results were obtained using the FS+ and FS− methods. The CC representation predicted by the ECP method agrees with those in the table.
[b]Coupling parameterization. See Sec. II for details.
[c]Initial conditions (E,j), where E is the total energy in eV, and j is the initial rotational state of the diatom. See Sec. III for details.

these 30 observables. For all the methods except the ECP method, the CC criterion predicts the most accurate representation overall (i.e., averaged over all six observables) for all five cases. We conclude that the CC representation is the most accurate representation for both surface hopping and decay of mixing calculations, even though surface hopping information is used as the criterion.

Average relative errors for the MXH and YRH systems as well as for the MCH systems are summarized in Table VIII. Errors for the YRH systems are taken directly from Ref. 89. Errors for the MXH systems were recomputed using the accurate quantum mechanical data from Ref. 82, and these errors differ from those presented elsewhere[89] because of a typographical error in the accurate quantal data used in Ref. 89. The error affected only one of the nine MXH cases.

As previously reported,[81] the CC representation is always the A representation for the YRH systems, and for these systems, the CC and A representations are systematically more accurate than D representation. For the MXH systems, the A representation is the least accurate representation for

TABLE VII. Relative errors (%) averaged over the five MCH cases.

Method	Rep[a]	P_R	P_Q	P_N	F_R	E'_{int}	E''_{int}	Probs[b]	Fracts[c]	Overall[d]
ECP	A	118	43	52	49	24	16	71	29	51
	D	98	152	54	39	22	8	101	23	62
	CC	108	119	49	43	24	4	92	24	58
FS−	A	116	76	58	38	19	13	84	24	54
	D	74	70	64	21	21	11	69	17	43
	CC	91	45	60	21	21	10	65	18	41
FS+	A	119	64	58	41	20	16	80	26	53
	D	76	68	63	17	24	8	69	16	43
	CC	88	44	58	20	24	6	63	17	40
FSTU∇V	A	122	81	52	48	20	13	85	27	56
	D	66	81	57	18	22	9	68	16	42
	CC	81	48	52	21	23	9	60	18	39
SE	A/D/CC	118	138	42	45	45	10	100	33	66
SCDM	A	56	111	37	18	25	17	68	20	44
	D	42	49	42	15	23	21	45	20	32
	CC	47	42	41	12	24	21	43	19	31
CSDM	A	51	98	39	19	24	19	63	21	42
	D	40	59	40	17	22	20	47	20	33
	CC	46	56	40	14	23	20	47	19	33

[a]Electronic representation; A=adiabatic, D=diabatic, and CC=Calaveras County.
[b]Average of the errors for P_R, P_Q, and P_N.
[c]Average of the errors for F_R, E'_{int}, and E''_{int}.
[d]Average of the errors for all six observables.

TABLE VIII. Average relative errors (%) for three YRH, nine MXH, and five MCH cases.

		YRH (weak coupling)			MXH (avoided crossing)			MCH (conical intersection)		
Method	Rep[a]	Probs[b]	Fracts[c]	Overall[d]	Probs	Fracts	Overall	Probs	Fracts	Overall
ECP	A	377	4	191	109	56	83	71	29	51
	D	1016	30	523	146	57	101	101	23	62
	CC	377	4	191	140	57	98	92	24	58
FS−	A	53	18	36	58	31	44	84	24	54
	D	723	49	386	42	19	31	69	17	43
	CC	53	18	36	54	30	42	65	18	41
FS+	A	43	15	29	67	39	53	80	26	53
	D	548	29	289	58	26	42	69	16	43
	CC	43	15	29	68	37	53	63	17	40
FSTU∇V	A	31	19	25	54	32	43	85	27	56
	D	230	26	128	35	19	27	68	16	42
	CC	31	19	25	47	30	38	60	18	39
SE	A/D/CC	e	e	e	109	39	74	100	33	66
SCDM	A	20	17	19	22	20	21	68	20	44
	D	69	22	46	21	18	20	45	20	32
	CC	20	17	19	24	19	22	43	19	31
CSDM	A	21	18	20	21	19	20	63	21	42
	D	41	22	32	20	18	19	47	20	33
	CC	21	18	20	24	19	21	47	19	33

[a]Electronic representation; A=adiabatic, D=diabatic, and CC=Calaveras County.
[b]Average of the errors for P_R, P_Q, and P_N.
[c]Average of the errors for F_R, E'_{int}, and E''_{int}.
[d]Average of the errors for all six observables.
[e]The SE method fails to predict any reactive or quenching trajectories for some YRH cases.

most surface hopping methods, the D representation is the most accurate representation, and the CC representation gives intermediate results. For the decay of mixing methods, all three representations give similar results for the MXH systems. Because the results are similar for the A and D representations for the MXH cases and the CC representation is the A representation for all of the YRH cases, the MCH cases provide a useful test of the CC criterion; as discussed above, the CC criterion is found to successfully predict the most accurate representation for the MCH systems.

Based on the YRH, MXH, and MCH results, one cannot conclude that the A representation is *always* the preferred representation for surface hopping or more generally for semiclassical trajectories. It is true, however, that when the A representation is preferred, errors using the D representation are typically larger than errors obtained using the A representation when the D representation is preferred, i.e., on average, using the A representation exclusively gives smaller errors than using the D representation exclusively. Therefore, in the total absence of information about a system, the A representation may be preferred. However, with a small amount of dynamical knowledge (obtained by running a small set of trajectories) one may compute the CC representation, which is found to be systematically more accurate than either the A or D representations, both in this study and previous work.[86–89] It is also reasonable to expect that for some systems and under certain conditions (such as high-energy collisions[91,162,163]), the D representation may be significantly more accurate than the A representation.

IV.B. Representation independence

Although the CC representation is the preferred representation for semiclassical trajectories, it is likely that many large systems may defy a one-representation description. Therefore, as noted above, one criterion for a successful semiclassical trajectory method is reduced dependence on the choice of electronic representation. For the surface hopping methods, the overall relative errors in the A and D representations differ on average by ~30% for MXH and ~25% for MCH. For the YRH cases, which are predicted to be strongly adiabatic by the CC criterion (see Table VI), the adiabatic and diabatic representations differ by factors of 4–10 for the surface hopping methods.

As noted above, the SE method is formally independent of electronic representation. Therefore, one may expect that methods based on the SE method (e.g., the SCDM and CSDM methods) will be less dependent on representation than surface hopping methods. For the MXH cases, the SCDM and CSDM methods give nearly identical errors in the A and D representations, and there is larger representation dependence for the MCH systems (30% and 20% for SCDM and CSDM, respectively). For the YRH cases, however, the SCDM and CSDM methods have much better representation independence than the surface hopping methods and have errors that differ by 80% and 50%, respectively. The most representation-independent method overall (aside from the SE method which has perfect representation independence) is the CSDM method. The CSDM method, in fact, was designed[89] to better reflect the true density matrix evolution contained in the representation-independent semiclassical Ehrenfest method, without having the drawbacks of the semiclassical Ehrenfest method.

IV.C. Accuracy for systems with conical intersections

Next, the relative overall accuracies of the semiclassical trajectory methods are considered, and attention is focused

on results obtained using the most accurate representation, i.e., the CC representation. Of the surface hopping methods (ECP, FS−, FS+, and FSTU∇V), the ECP method is the least accurate method with an average overall error of 58%. The ECP method differs from the three other methods (FS−, FS+, and FSTU∇V) in three significant ways. First, it uses a hopping probability based on integrating the classical path equations coherently through regions of strong coupling, whereas the other methods use a local hopping probability. We have previously found that including regions of extended coherence within the DM formalism (as in the CSDM method) leads to improved results,[89] and this aspect of the ECP method may therefore be desirable. Second, surface hops are allowed in the ECP algorithm only at regions of maximal coupling. The other surface hopping methods allow surface hops whenever the electronic state populations are changing. Third, in the ECP method, the electronic state populations are reinitialized after each strong coupling region, whereas in the other methods they are not. We have not investigated which one of these differences causes the ECP method to be systematically worse than the methods based on the fewest-switches formalism.

The FS−, FS+, and FSTU∇V methods differ only in their treatment of frustrated hops. For the MCH systems, all three methods give similar results (with overall errors of ~40%), and the FSTU∇V method is slightly more accurate. For these cases, the number of successful hops is generally greater than the number of frustrated hops when the CC representation is used (see Table VI), although the FSTU∇V method does feature a fairly significant number of nonlocal hops (2%–30% of trajectories experience at least one nonlocal hop). Nonetheless, the similar errors for all three methods indicate that the treatment of frustrated hops is not the dominant source of error for these systems. (The treatment of frustrated hops is more significant in weak coupling cases such as the YRH model systems.[83,84])

As noted above, the SE method has the desirable feature that it is independent of electronic representation. Unfortunately, it is the least accurate method for the MCH cases with an overall error of 66%. The DM formalism has been developed to retain the desirable features of the SE method, while also incorporating surface-hopping-like physical final states. For the MCH systems, the SCDM and CSDM methods (with average errors of 31% and 33%, respectively) are twice as accurate as the SE method and more accurate than the surface hopping methods. The CSDM method, as mentioned above, is also less dependent on the choice of electronic representation (or, equivalently, the CSDM is more accurate than the other methods when the non-CC representation is used), and therefore we conclude that the CSDM method is the preferred semiclassical trajectory method for systems with conical intersections.

These conclusions agree with earlier studies on the YRH and MXH systems[87,89] (summarized in Table VIII). There and here, the DM methods are both more accurate and less representation dependent than the surface hopping methods, and while the SCDM and CSDM method have similar errors when the CC representation is used, the CSDM method is the least representation dependent of all the methods tested. It is very encouraging that our conclusions drawn on the basis of more weakly coupled YRH and MXH systems continue to hold for the more strongly coupled MCH systems. The CSDM method is therefore confirmed as the preferred semiclassical trajectory method overall.

IV.D. The behavior of semiclassical trajectories near conical intersections

In addition to providing an efficient means of modeling large photochemical systems, semiclassical trajectories also provide a means of studying chemical events in mechanistic detail. This is especially interesting in the context of conical intersections, where one can ask questions about what role the CI plays in the nonadiabatic event. Therefore, we present a general discussion of the behavior of semiclassical trajectories near conical intersections.

Using the FSTU∇V and CSDM methods, we gathered various statistics for the MCH cases. The trends for each of the five cases are similar, and a detailed study is presented for the SL parameterization only. We also consider the SL parameterization of the MXH system for comparison. Note that the MXH and MCH systems have identical diabatic potential energy surfaces and differ only in their coupling; the MXH system has an avoided crossing (AC), and the MCH system has a CI. For both cases, the (1.1,0) initial conditions and identical numerical parameters for trajectory integration are used.

Conical intersections are often implicated in experimentally observed ultrafast (femtosecond) decay mechanisms. To study this issue, the average delay time T_{D} for each trajectory was computed as follows:[164]

$$T_D = T - R^i_{\mathrm{rel}}/V^i_{\mathrm{rel}} - R^f_{\mathrm{rel}}/V^f_{\mathrm{rel}}, \tag{18}$$

where T is the total time for the scattering event, and R^x_{rel} and V^x_{rel} are the initial ($x=``i"$) and final ($x=``f"$) relative center-of-mass distances and velocities, respectively, of the atom-diatom fragments. The delay time is often negative for these systems, as a consequence of the small-R_{rel} regions excluded by the repulsive potential at small internuclear distances.[165]

Histogram plots of T_D for both the MXH (AC) and MCH (CI) SL parameterizations are shown in Fig. 4. The one-standard-deviation (1σ) Monte Carlo error bars for the bins in Fig. 4 are less than 0.005. For the CSDM method [Figs. 4(a) and 4(b)], the distributions of T_D obtained using the diabatic and adiabatic representations agree well with each other, whereas the distributions for the FSTU∇V method agree less well with each other. The diabatic FSTU∇V results (which were shown to be more accurate in Sec. IV.C) agree with the CDSM results for reactive trajectories, but not for quenching trajectories. In general, the MXH system has shorter (more negative, faster) delay times than the MCH systems. The differences between the delay times for the MXH and MCH systems are not dramatic, however.

This result may be compared with a wave packet study by Stock and co-workers,[67] where two-dimensional CI and AC models were used to study excited-state decay. They found that when the 2D system was coupled to an external

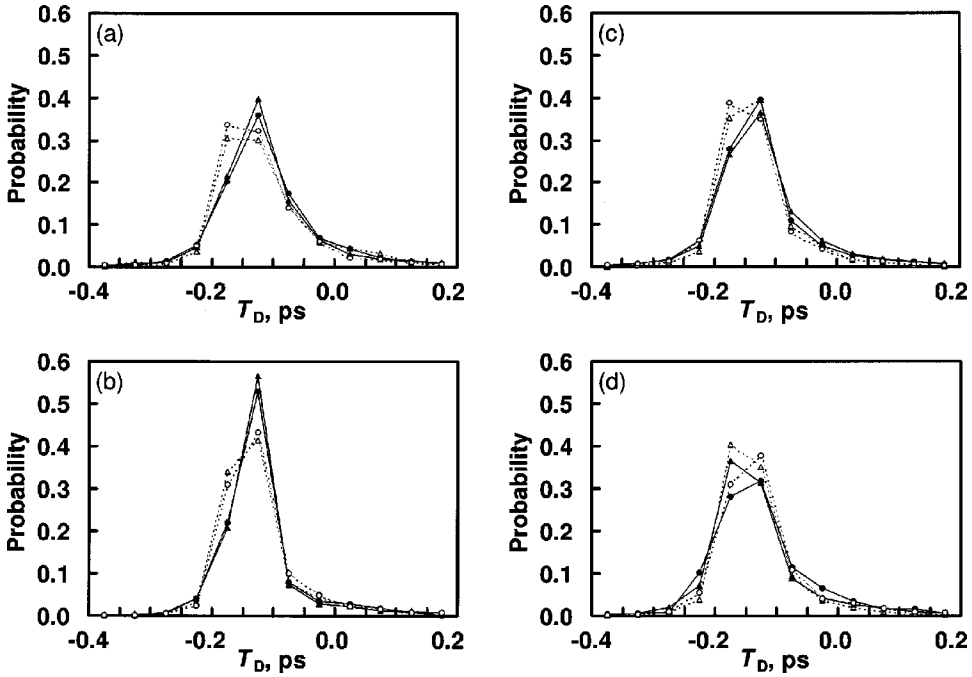

FIG. 4. Delay times for SL parameterizations of the MCH (solid) and MXH (dashed) systems and for the (1.1,0) initial conditions for the adiabatic (triangles) and diabatic (circles) representations. Results for the CSDM method are shown in panels (a) and (b), and results for the FSTU∇V method are shown in panels (c) and (d). Panels (a) and (c) show reactive trajectories, and panels (b) and (d) show quenching trajectories.

bath, the CI system decayed much faster than the AC system, and they observed and cited two reasons: (i) the CI captured the wave packet more readily than the AC, and (ii) the CI more efficiently disposed of the wave packet after de-excitation. This behavior has been anticipated and demonstrated elsewhere.[123,124] When the 2D models were treated as isolated systems (uncoupled to the bath), the CI and AC systems displayed similar dynamics.

For the MCH systems, two degrees of freedom represent the plane of the cone, and there is one additional ''external'' degree of freedom. It is interesting that this situation seems to more closely resemble the uncoupled 2D model than the coupled 2D model. For larger systems with more degrees of freedom, the dynamical differences between the CI and AC may become more pronounced. However, with more degrees of freedom, there is also an increased probability that the system may go ''around'' or ''past'' the cone, and it is not clear how these effects compete for real systems. Furthermore, the 2D model CI that was studied[74] was upright and symmetric, as opposed to the sloped and asymmetric cone that appears in the MCH systems. As mentioned above, upright cones are expected to more efficiently funnel wave packets to the ground state than sloped cones.

It is interesting to study the two sources of enhanced CI decay identified above more closely for the MCH and MXH systems. To separate the two processes more clearly, the time of the first and last hopping events $T_h^{(1)}$ and $T_h^{(N)}$ are used to indicate the beginning and end of the interaction with the CI or AC, respectively, and to define a set of three times t_C, t_I, and t_D. The half-reaction delay times t_C and t_D correspond to the capture and disposal processes identified above, and t_I is the time spent interacting with the CI or AC:

$$t_C = T_h^{(1)} - R_{\mathrm{rel}}^i / V_{\mathrm{rel}}^i, \tag{19}$$

$$t_I = T_h^{(N)} - T_h^{(1)}, \tag{20}$$

and

$$t_D = T - T_h^{(N)} - R_{\mathrm{rel}}^f / V_{\mathrm{rel}}^f, \tag{21}$$

where $T_D = t_C + t_I + t_D$. Due to the stochastic nature of the surface hopping algorithm, only the ensemble averaged distributions of values of these quantities are meaningful. Note that these definitions are not suitable for the diabatic representation where trajectories may de-excite without hopping.

Table IX summarizes the average values of T_D, t_C, t_I, and t_D for reactive and quenching trajectories for the SL parameterizations of the MCH and MXH systems using the adiabatic representation and the FSTU∇V method. The average capture time t_C is similar for both systems and for both kinds of events. The scattering trajectories have total energies of 1.1 eV, and both the energy of the MCH CI and the energy of the excited state where the MXH energy gap is a minimum is ~0.6 eV. Therefore, for both systems, the trajectories have significant kinetic energy near the strong cou-

TABLE IX. Average delay times (fs) for the SL parameterizations of the MXH (AC) and MCH (CI) systems.[a]

Final arrangement	System	$\langle T_D \rangle$, fs	$\langle t_C \rangle$, fs	$\langle t_I \rangle$, fs	$\langle t_D \rangle$, fs
Reactive	CI	−125	−123	39	−41
	AC	−137	−123	22	−36
Quenching	CI	−117	−129	56	−44
	AC	−119	−126	37	−30

[a]FSTU∇V calculations in the adiabatic representation.

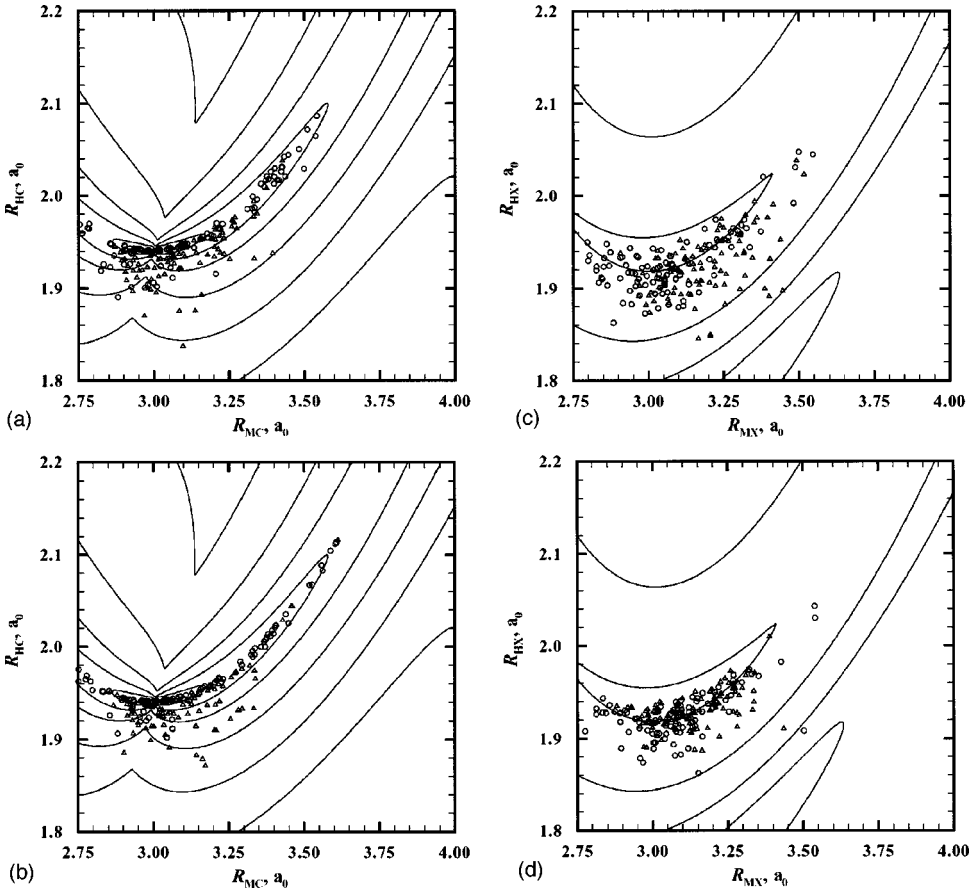

FIG. 5. Contour plot of d with contour spacings 0.15, 0.5, 1.5, 5, 15, and $50\,a_0^{-1}$ for the SL parameterizations of (a,b) MCH and (c,d) MXH. The maximum contour for the MXH system is $5\,a_0^{-1}$. Also shown are the geometries of maximum d for 100 reactive (circles) and 100 quenching (triangles) CSDM trajectories propagated in the (a,c) adiabatic and (b,d) diabatic representations.

pling region, and they do not have to rely on the shape of the excited surface to draw them toward the strong coupling region. The capture effect that was observed in the 2D study discussed above was for a system with small (0 K) initial kinetic energy, where one would expect this effect to be more significant.

There is a difference in the dynamics of the MXH and MCH systems after the first surface hop. Our results confirm that there is enhanced disposal of the trajectories after the nonadiabatic event, but with a difference in t_D of only $\sim$10 fs. The trajectories interact with the CI for $\sim$18 fs longer than with the AC, and these two effects have opposite effects on the overall delay time T_D. One may justify the increase interaction time t_I by noting that the smaller energy gap near the CI creates a larger region of significant coupling than for the AC system.

The magnitudes of these effects are small and will depend on a variety of factors including the shape of the CI and the conditions of the dynamics, and one must be careful interpreting such small differences in the times for these model systems. Furthermore, it may be more appropriate to define the capture and disposal times based on criteria other than hopping. As we are interested in only a qualitative dynamical picture of the behavior of semiclassical trajectories near CIs, we do not pursue a more detailed study of these processes, but the discussion above is useful for understanding the caution that the presence of a CI need not cause a qualitative difference in the dynamics.

Next, we consider how the semiclassical trajectories behave as they ''funnel down'' near the CI. In the simplest model of dynamics near a CI, systems are depicted as deexciting directly via a steepest-descent path through the cone. In Fig. 5, contour plots of the magnitude d of the nonadiabatic coupling **d** for collinear geometries are shown, along with the geometries where the maximum value $d_{\max}$ of d is attained along 100 reactive and 100 quenching CSDM trajectories. (Note: The trajectories were not constrained to collinear geometries, so the correlation between the contours and the magnitude of d at the circles and diamonds is only approximate.) The maximum of d along a particular trajectory represents the closest point along that trajectory to the cone. Figure 5 shows similar trends in the adiabatic and diabatic representations; therefore, in the remainder of this section only the diabatic results are discussed.

For the MCH system [Figs. 5(a) and 5(b)], only 10% of all trajectories have a $d_{\max}$ of less than $15\,a_0^{-1}$, and only 4% have a $d_{\max}$ of less than $5\,a_0^{-1}$. The median value of $d_{\max}$ is $\sim 50\,a_0^{-1}$. The seam of conical intersection is located at $R_{\mathrm{HC}} \approx 1.94\,a_0$ and $R_{\mathrm{MC}} \approx 3.00\,a_0$ for M–C–H bond angles from 100° to 180°. The average values and one-σ standard deviations of these distances at $d_{\max}$ (for all trajectories) is

1.96 ± 0.04 and $3.18 \pm 0.39\, a_0$, respectively. The distribution is wider along R_{MC} [which has a sloped shape, see Fig. 3(b)] than along R_{HC} [which has a peaked shape, see Fig. 3(b)].

For the MXH system [Figs. 5(c) and 5(d)], the maximum value of d is $\sim 6\, a_0^{-1}$, and the median value of d_{max} is $\sim 5\, a_0^{-1}$. Comparing the distributions of the locations of d_{max} for the MXH and MCH systems, it can be seen that the CI focuses the distribution of d_{max} along R_{HC} but not along R_{MC}. One would expect less focusing along R_{MC} because the cone in MCH systems is sloped in this direction. Furthermore, as discussed above, because of the significant kinetic energy of the trajectories, the nuclear motion is likely not as sensitive to the shape of the surfaces near the cone as, for example, in those low-temperature photodissociation processes where the Franck–Condon region is not significantly higher in energy than the CI.

Finally, we note that for the MCH system, 84% of quenching trajectories have a d_{max} of at least $15\, a_0^{-1}$, whereas 98% of reactive trajectories have a d_{max} in this range, indicating a greater preference for trajectories to react the more closely they pass by the cone.

V. CONCLUDING REMARKS

A family of five atom–diatom model systems was presented, and each system features a seam of conical intersections. Accurate quantum dynamics calculations were carried out and used to test the performance of several surface hopping methods, the semiclassical Ehrenfest method, and two decay of mixing (DM) methods. The DM formalism is more accurate than the surface hopping formalism; the best surface hopping method (FSTU∇V) and the best DM methods (SCDM and CSDM) have overall relative errors of 40% and ~30%, respectively. Furthermore, the CSDM method is less dependent on the choice of electronic representation than the other methods making it the preferred semiclassical trajectory method for systems with conical intersections.

These conclusions agree with the results of previous tests[87,89] using a set of systems with avoided crossings and weak coupling cases, and they add confidence to our recommendation of the CSDM method for modeling coupled-states dynamics.

The diabatic representation was shown to be the most accurate representation for four of the five newly presented systems, and the Calaveras County criterion for determining which representation is more accurate was successfully applied in every case.

Finally, an analysis of the behavior of semiclassical trajectories near conical intersections was presented. It was found that the sloped cones in the present study do not significantly enhance decay (as compared with a similar system with an avoided crossing) but do affect product branching.

ACKNOWLEDGMENTS

The authors are grateful to Chaoyuan Zhu and Shkiha Nangia for many useful contributions to our research in this area. This work was supported in part by the National Science Foundation under Grant No. CHE03-49122.

[1] G. Herzberg, *Molecular Spectra and Molecular Structure III. Electronic Spectra and Electronic Structure of Polyatomic Molecules* (Van Nostrand Reinhold, New York, 1966), pp. 442ff.
[2] D. R. Yarkony, J. Phys. Chem. A **105**, 985 (1996).
[3] G. A. Worth and L. S. Cederbaum, Annu. Rev. Phys. Chem. **55**, 127 (2004).
[4] H. E. Zimmerman and R. E. Factor, J. Am. Chem. Soc. **102**, 3538 (1980).
[5] V. Bonacic-Koutecky, J. Koutecky, and J. Michl, Angew. Chem., Int. Ed. Engl. **26**, 107 (1987).
[6] L. J. Butler, Annu. Rev. Phys. Chem. **49**, 125 (1998).
[7] E. W.-G. Diau, S. De Feyter, and A. H. Zewail, J. Chem. Phys. **110**, 9785 (1999).
[8] N. R. Forde, M. L. Morton, S. L. Curry, S. J. Wrenn, and L. J. Butler, J. Chem. Phys. **111**, 4558 (1999).
[9] C. Mirianas and A. H. Zewail, J. Phys. Chem. A **103**, 7408 (1999).
[10] A. Bach, J. M. Hutchinson, R. J. Holiday, and F. F. Crim, J. Phys. Chem. A **107**, 10490 (2003).
[11] W. Fuß, W. Rettig, W. E. Schmid, S. A. Trushin, and T. Yatsuhashi, Faraday Discuss. **124**, 23 (2004).
[12] J. Wei, J. Riedel, A. Kuczmann, F. Renth, and F. Temps, Faraday Discuss. **127**, 267 (2004).
[13] E. Teller, J. Phys. Chem. **41**, 109 (1937).
[14] D. G. Truhlar and C. A. Mead, Phys. Rev. A **68**, 032501 (2003).
[15] D. G. Truhlar, Faraday Discuss. **127**, 242 (2004).
[16] M. J. Bearpark, M. A. Robb, and H. B. Schlegel, Chem. Phys. Lett. **223**, 269 (1994).
[17] M. R. Manaa and D. R. Yarkony, J. Am. Chem. Soc. **116**, 11444 (1994).
[18] F. Bernardi, M. Olivucci, and M. A. Robb, Chem. Soc. Rev. **25**, 321 (1996).
[19] D. R. Yarkony, Rev. Mod. Phys. **68**, 985 (1996); D. R. Yarkony, J. Phys. Chem. A **108**, 3200 (2004); Faraday Discuss. **127**, 325 (2004).
[20] A. Toniolo, M. Ben-Nun, and T. J. Martinez, J. Phys. Chem. A **106**, 4679 (2002).
[21] R. N. Porter, R. M. Stephens, and M. Karplus, J. Chem. Phys. **49**, 5163 (1968).
[22] A. J. C. Varandas, F. B. Brown, C. A. Mead, D. G. Truhlar, and N. C. Blais, J. Chem. Phys. **86**, 6258 (1987).
[23] A. Kuppermann and Y.-S. M. Yu, Chem. Phys. Lett. **205**, 577 (1993).
[24] A. Ravinder, A. Shaw, A. Kuppermann, and D. R. Yarkony, J. Chem. Phys. **115**, 4640 (2001).
[25] M. A. Robb, F. Bernardi, and M. Olivucci, Pure Appl. Chem. **67**, 783 (1985).
[26] V. Bonacic-Koutecky, K. Schoffel, and J. Michl, Theor. Chim. Acta **72**, 459 (1987).
[27] A. L. Sobolewski, C. Woywod, and W. Domcke, J. Chem. Phys. **98**, 5627 (1993).
[28] M. Klessinger, Angew. Chem. **107**, 597 (1995).
[29] F. Bernardi, M. Olivucci, and M. A. Robb, Chem. Soc. Rev. **1996**, 321 (1996).
[30] D. R. Yarkony, J. Phys. Chem. **100**, 18612 (1996).
[31] G. A. Worth and L. S. Cederbaum, Chem. Phys. Lett. **338**, 219 (2001).
[32] M. Garavelli, F. Bernardi, M. A. Robb, and M. Olivucci, Int. J. Photoenergy **4**, 57 (2002).
[33] A. Migani, A. Sinicropi, N. Ferré, A. Cembran, M. Garavelli, and M. Ollivucci, Faraday Discuss. **127**, 179 (2004).
[34] A. Aguado, C. Suárez, and M. Paniagua, J. Chem. Phys. **98**, 308 (1991).
[35] P. Halvick and D. G. Truhlar, J. Chem. Phys. **96**, 2895 (1992).
[36] Y. Amatatsu, S. Yabushita, and K. Morokuma, J. Chem. Phys. **100**, 4894 (1994).
[37] V. D. Vachev, J. H. Frederick, B. A. Grishanin, V. N. Zadkov, and N. I. Koroteev, J. Phys. Chem. **99**, 5247 (1995).
[38] M. S. Topaler, D. G. Truhlar, X. Y. Chang, P. Piecuch, and J. C. Polanyi, J. Chem. Phys. **108**, 5349 (1998).
[39] A. J. Dobbyn, J. N. L. Connor, N. A. Besley, P. J. Knowler, and G. C. Schatz, Phys. Chem. Chem. Phys. **1**, 959 (1999).
[40] P. Cattaneo and M. Persico, Theor. Chem. Acc. **103**, 390 (2000).
[41] A. W. Jasper, M. D. Hack, D. G. Truhlar, and P. Piecuch, J. Chem. Phys. **116**, 8353 (2002).
[42] R. P. Krawczyk, A. Viel, U. Manthe, and W. Domcke, J. Chem. Phys. **119**, 1397 (2003).
[43] D. G. Truhlar, J. W. Duff, N. C. Blais, J. C. Tully, and B. C. Garrett, J. Chem. Phys. **77**, 764 (1982).
[44] S. Klein, M. J. Bearpark, B. R. Smith, and M. A. Robb, Chem. Phys. Lett. **292**, 259 (1998).

[45] M. Devmal, M. J. Bearpark, B. R. Smith, M. Olivucci, F. Bernardi, and M. A. Robb, J. Org. Chem. **63**, 4594 (1998).
[46] M. Ben-Nun and T. J. Martinez, Chem. Phys. **259**, 237 (2000).
[47] M. Hartmann, J. Pittner, and V. Bonacic-Koutecky, J. Chem. Phys. **114**, 2123 (2001).
[48] G. Granucci, M. Persico, and A. Toniolo, J. Chem. Phys. **114**, 10608 (2001).
[49] N. L. Doltsinis and D. Marx, Phys. Rev. Lett. **88**, 166402 (2002).
[50] N. L. Doltsinis and D. Marx, J. Theor. Comp. Chem. **1**, 319 (2002).
[51] K. K. Baeck and T. J. Martinez, Chem. Phys. Lett. **375**, 299 (2003).
[52] S. L. Mielke, G. J. Tawa, D. G. Truhlar, and D. W. Schwenke, J. Am. Chem. Soc. **115**, 6436 (1993).
[53] S. L. Mielke, G. J. Tawa, D. G. Truhlar, and D. W. Schwenke, Int. J. Quantum Chem., Quantum Chem. Symp. **27**, 621 (1993).
[54] T. C. Allision, S. L. Mielke, D. W. Schwenke, and D. G. Truhlar, J. Chem. Soc., Faraday Trans. **93**, 825 (1997).
[55] M. S. Topaler, T. C. Allison, D. W. Schwenke, and D. G. Truhlar, J. Chem. Phys. **109**, 3321 (1998); **110**, 687(E) (1999); **113**, 3928(E) (2000).
[56] M. D. Hack, A. W. Jasper, Y. L. Volobuev, D. W. Schwenke, and D. G. Truhlar, J. Phys. Chem. A **103**, 6309 (1999).
[57] M. D. Hack, A. W. Jasper, Y. L. Volobuev, D. W. Schwenke, and D. G. Truhlar, J. Phys. Chem. A **104**, 217 (2000).
[58] F. Santoro, C. Petrongolo, G. Granucci, and M. Persico, Chem. Phys. **259**, 193 (2000); **261**, 489(E) (2000).
[59] H. Köppel, M. Doscher, and S. Mahapatra, Int. J. Quantum Chem. **80**, 942 (2000).
[60] S. Mahaptra, H. Köppel, and L. S. Cederbaum, J. Phys. Chem. A **105**, 2321 (2001).
[61] J. C. Juanes-Marcos and S. C. Althorpe, Chem. Phys. Lett. **381**, 743 (2003).
[62] B. K. Kendrick, J. Chem. Phys. **114**, 8796 (2001); **118**, 10502 (2003).
[63] G. A. Worth, H.-D. Meyer, and L. S. Cederbaum, J. Chem. Phys. **109**, 3518 (1998).
[64] A. Raab, G. A. Worth, H.-D. Meyer, and L. S. Cederbaum, J. Chem. Phys. **110**, 936 (1999).
[65] C. Cattarius, G. A. Worth, H.-D. Meyer, and L. S. Cederbaum, J. Chem. Phys. **115**, 2088 (2001).
[66] S. Mahapatra, G. A. Worth, H.-D. Meyer, L. S. Cederbaum, and H. Köppel, J. Phys. Chem. A **105**, 5567 (2001).
[67] G. A. Worth and L. S. Cederbaum, Chem. Phys. Lett. **348**, 477 (2001).
[68] H. Köppel, M. Döscher, I. Bâldea, H.-D. Meyer, and P. G. Szalay, J. Chem. Phys. **117**, 2657 (2002).
[69] G. A. Worth, P. Hunt, and M. A. Robb, J. Phys. Chem. A **107**, 621 (2003).
[70] V. Vallet, Z. Lan, S. Mahapatra, A. L. Sobolewski, and W. Domcke, Faraday Discuss. **127**, 283 (2004).
[71] A. Alijah and E. E. Nikitin, Mol. Phys. **96**, 1399 (1999).
[72] A. Ferretti, A. Lami, and G. Villani, Chem. Phys. **259**, 201 (2000).
[73] J. Li and C. Woywod, Chem. Phys. Lett. **327**, 128 (2003).
[74] B. Balzer, S. Hahn, and G. Stock, Chem. Phys. Lett. **379**, 351 (2003).
[75] M. S. Topaler, M. D. Hack, T. C. Allison, Y.-P. Liu, S. L. Mielke, D. W. Schwenke, and D. G. Truhlar, J. Chem. Phys. **106**, 8699 (1997).
[76] M. Ben-Nun and T. J. Martinez, Chem. Phys. Lett. **298**, 57 (1998).
[77] M. S. Topaler, T. C. Allison, D. W. Schwenke, and D. G. Truhlar, J. Phys. Chem. **102**, 1666 (1998).
[78] M. Thoss, W. H. Miller, and G. Stock, J. Chem. Phys. **112**, 10282 (2000).
[79] M. J. Paterson, P. A. Hunt, M. A. Robb, and O. Takahashi, J. Phys. Chem. A **106**, 10494 (2002).
[80] N. C. Blais and D. G. Truhlar, J. Chem. Phys. **79**, 1334 (1983).
[81] M. D. Hack and D. G. Truhlar, J. Phys. Chem. A **104**, 7917 (2000).
[82] Y. L. Volobuev, M. D. Hack, M. S. Topaler, and D. G. Truhlar, J. Chem. Phys. **112**, 9716 (2000).
[83] A. W. Jasper, M. D. Hack, and D. G. Truhlar, J. Chem. Phys. **115**, 1804 (2001).
[84] A. W. Jasper, S. N. Stechmann, and D. G. Truhlar, J. Chem. Phys. **116**, 5424 (2002); **117**, 10427(E) (2002).
[85] A. W. Jasper and D. G. Truhlar, Chem. Phys. Lett. **369**, 60 (2003).
[86] C. Zhu, A. W. Jasper, and D. G. Truhlar, J. Chem. Phys. **120**, 5543 (2004).
[87] A. W. Jasper, C. Zhu, S. Nangia, and D. G. Truhlar, Faraday Discuss. **127**, 1 (2004).
[88] A. W. Jasper, B. K. Kendrick, C. A. Mead, and D. G. Truhlar, in *Modern Trends in Chemical Reaction Dynamics, Part I*, edited by X. Yang and K. Liu (World Scientific, Singapore, 2004), pp. 329–392.
[89] C. Zhu, S. Nangia, A. W. Jasper, and D. G. Truhlar, J. Chem. Phys. **121**, 7658 (2004).
[90] J. C. Tully, in *Dynamics of Molecular Collisions, Part B*, edited by W. H. Miller (Plenum, New York, 1976), pp. 217–267.
[91] M. S. Child, in *Atom–Molecule Collision Theory*, edited by R. B. Bernstein (Plenum, New York, 1979), pp. 427–465.
[92] D. G. Truhlar and J. T. Muckerman, in *Atom–Molecule Collision Theory*, edited by R. B. Bernstein (Plenum, New York, 1979), pp. 505–566.
[93] S. Chapman, Adv. Chem. Phys. **82**, 423 (1992).
[94] J. C. Tully, Faraday Discuss. **110**, 407 (1998).
[95] L. D. Landau, Phys. Z. Sowjetunion **2**, 46 (1932).
[96] C. Zener, Proc. R. Soc. London, Ser. A **137**, 696 (1932).
[97] E. Teller, J. Chem. Phys. **41**, 109 (1937).
[98] N. Rosen and C. Zener, Phys. Rev. **40**, 502 (1932).
[99] Yu. N. Demkov, J. Exp. Theor. Phys. **45**, 195 (1963); Sov. Phys. JETP **18**, 138 (1964).
[100] Yu. N. Demkov, Dokl. Akad. Nauk SSSR **166**, 1076 (1966); Sov. Phys. Dokl. **11**, 138 (1966).
[101] R. Alimi, R. B. Gerber, A. D. Hammerich, R. Kosloff, and M. A. Ratner, J. Chem. Phys. **93**, 6484 (1990).
[102] T. J. Martinez, M. Ben-Nun, and R. D. Levine, J. Phys. Chem. **100**, 7884 (1996); **101**, 6839 (1997).
[103] J. C. Burant and J. C. Tully, J. Chem. Phys. **112**, 6097 (2000).
[104] S. Nielsen, R. Kapral, and G. Ciccotti, J. Chem. Phys. **112**, 6543 (2000).
[105] A. Donoso, D. Kohen, and C. C. Martens, J. Chem. Phys. **112**, 7345 (2000).
[106] M. D. Hack, A. M. Wensmann, D. G. Truhlar, M. Ben-Nun, and T. J. Martinez, J. Chem. Phys. **115**, 1172 (2001).
[107] A. Donoso and C. C. Martens, Int. J. Quantum Chem. **90**, 1348 (2002).
[108] C.-C. Wan and J. Schofield, J. Chem. Phys. **116**, 494 (2002).
[109] K. Ando and M. Santer, J. Chem. Phys. **118**, 10399 (2003).
[110] A. Sergi, D. MacKernan, G. Cicotti, and R. Kapral, Theor. Chem. Acc. **110**, 49 (2003).
[111] B. C. Garrett, M. J. Redman, D. G. Truhlar, and C. F. Melius, J. Chem. Phys. **74**, 412 (1981).
[112] F. X. Gadea, H. Berriche, O. Roncero, P. Villarial, and G. D. Barrio, J. Chem. Phys. **107**, 10515 (1997).
[113] A. Kuppermann, in *Dynamics of Molecules and Chemical Reactions*, edited by R. E. Wyatt and J. Z. H. Zhang (Dekker, New York, 1996), pp. 411–472.
[114] D. R. Yarkony, J. Phys. Chem. A **105**, 6277 (2001).
[115] C. A. Mead and D. G. Truhlar, J. Chem. Phys. **77**, 6090 (1982).
[116] B. K. Kendrick, C. A. Mead, and D. G. Truhlar, Chem. Phys. Lett. **330**, 629 (2000).
[117] B. K. Kendrick, C. A. Mead, and D. G. Truhlar, Chem. Phys. **277**, 31 (2002).
[118] A. W. Jasper, M. D. Hack, D. G. Truhlar, and P. Piecuch, J. Chem. Phys. **116**, 8353 (2002).
[119] S. Sato, J. Chem. Phys. **23**, 2465 (1955).
[120] J. K. Cashion and D. R. Herschbach, J. Chem. Phys. **40**, 2358 (1964).
[121] K. J. Laidler and J. C. Polanyi, Prog. React. Kinet. **3**, 1 (1965).
[122] P. J. Kuntz, E. M. Nemeth, J. C. Polanyi, S. D. Rosner, and C. E. Young, J. Chem. Phys. **44**, 1168 (1966).
[123] G. J. Atchity, S. S. Xantheas, and K. Ruedenberg, J. Chem. Phys. **95**, 1862 (1991).
[124] D. R. Yarkony, J. Chem. Phys. **114**, 2601 (2001).
[125] L. Schlessinger, Phys. Rev. **167**, 1411 (1968).
[126] J. Nuttall and H. L. Cohen, Phys. Rev. **188**, 1542 (1969).
[127] Y. Sun, D. J. Kouri, D. G. Truhlar, and D. W. Schwenke, Phys. Rev. A **41**, 4857 (1990).
[128] D. W. Schwenke, S. L. Mielke, and D. G. Truhlar, Theor. Chim. Acta **79**, 241 (1991).
[129] G. J. Tawa, S. L. Mielke, D. G. Truhlar, and D. W. Schwenke, in *Advances in Molecular Vibrations and Collisional Dynamics*, edited by J. M. Bowman (JAI, Greenwich, 1994), Vol. 2B, pp. 45–116.
[130] D. W. Schwenke, Y. L. Volobuev, S. L. Mielke *et al.*, VP, version 18.8 (University of Minnesota, Minneapolis, 1999).
[131] G. Herzberg and H. C. Longuet-Higgins, Discuss. Faraday Soc. **35**, 77 (1963).
[132] H. C. Longuet-Higgins, Proc. R. Soc. London, Ser. A **344**, 147 (1975).
[133] C. A. Mead and D. G. Truhlar, J. Chem. Phys. **70**, 2284 (1979).
[134] C. A. Mead, Chem. Phys. **49**, 23 (1980); Rev. Mod. Phys. **64**, 51 (1992).
[135] M. V. Berry, Proc. R. Soc. London, Ser. A **392**, 45 (1984).

[136] *Geometric Phases in Physics*, edited by A. Shapere and F. Wilczek (World Scientific, Singapore, 1989).
[137] A. Bohm, L. J. Boya, and B. Kendrick, Phys. Rev. A **43**, 1206 (1991).
[138] N. C. Blais and D. G. Truhlar, J. Chem. Phys. **79**, 1334 (1983).
[139] J. C. Tully, J. Chem. Phys. **93**, 1061 (1990).
[140] A. Bjerre and E. E. Nikitin, Chem. Phys. Lett. **1**, 179 (1967).
[141] J. C. Tully and R. K. Preston, J. Chem. Phys. **55**, 562 (1971).
[142] S. Hammes-Schiffer and J. C. Tully, J. Chem. Phys. **101**, 4657 (1994).
[143] U. Mller and G. Stock, J. Chem. Phys. **107**, 6230 (1997).
[144] W. H. Miller and T. F. George, J. Chem. Phys. **56**, 5637 (1972).
[145] G. Parlant and E. A. Gislason, J. Chem. Phys. **91**, 4416 (1989).
[146] H.-D. Meyer and W. H. Miller, J. Chem. Phys. **72**, 2272 (1980).
[147] D. A. Micha, J. Chem. Phys. **78**, 7138 (1983).
[148] M. Amarouche, F. X. Gadea, and J. Durup, Chem. Phys. **130**, 145 (1989).
[149] A. Garcia-Vela, R. B. Gerber, and D. G. Imre, J. Chem. Phys. **97**, 7242 (1992).
[150] O. V. Prezhdo and P. J. Rossky, J. Chem. Phys. **107**, 825 (1997).
[151] E. R. Bittner and P. J. Rossky, J. Chem. Phys. **107**, 8611 (1997).
[152] H. Wang, M. Thoss, and W. H. Miller, J. Chem. Phys. **115**, 2979 (2001).
[153] M. D. Hack and D. G. Truhlar, J. Chem. Phys. **114**, 9305 (2001).
[154] G. A. Fiete and E. J. Heller, Phys. Rev. A **68**, 022112 (2003).
[155] L. Turi and P. J. Rossky, J. Chem. Phys. **120**, 3688 (2004).
[156] C. Zhu, S. Nangia, A. W. Jasper *et al.*, NAT, version 8.1 (University of Minnesota, Minneapolis, 2004).
[157] T. Pacher, C. A. Mead, L. S. Cederbaum, and H. Köppel, J. Chem. Phys. **91**, 7057 (1989).
[158] R. G. Sadygov and D. R. Yarkony, J. Chem. Phys. **109**, 20 (1998).
[159] A. Thiel and H. Köppel, J. Chem. Phys. **110**, 9371 (1999).
[160] H. Köppel, J. Gronki, and S. Mahapatra, J. Chem. Phys. **115**, 2377 (2001).
[161] W. H. Zurek, Phys. Rev. D **24**, 1516 (1981).
[162] E. E. Nikitin and S. Y. Umanskii, *Theory of Slow Atomic Collisions* (Springer-Verlag, Heidelberg, 1984), p. 79.
[163] M. F. Herman, J. Chem. Phys. **111**, 10427 (1999).
[164] J. W. Duff and D. G. Truhlar, Chem. Phys. **4**, 1 (1974).
[165] B. C. Garrett, D. G. Truhlar, R. S. Grev, G. C. Schatz, and R. B. Walker, J. Phys. Chem. **85**, 3806 (1981).